

Simulating the transport and dispersal of volcanic ash clouds with initial conditions created by a 3D plume model

Zhixuan Cao^{1,2} Marcus Bursik³ Qingyuan Yang^{4,5} Abani Patra^{*,1,6}

¹ Mechanical and Aerospace Engineering Department, SUNY Buffalo, Buffalo, NY, USA

² Fluids Business Unit, ANSYS Inc, Lebanon, NH, USA

³ Center for Geohazards Studies, SUNY Buffalo, Buffalo, NY, USA

⁴ Earth Observatory of Singapore, Singapore, Singapore

⁵ The Asian School of the Environment, Nanyang Technological University, Singapore, Singapore

⁶ Data Intensive Studies Center, Tufts University, Medford, MA, USA

Correspondence*:

Abani Patra

abani.patra@tufts.edu

2 ABSTRACT

volcanic ash transport and dispersion (VATD) models simulate atmospheric transport of ash starting from a source originating at the volcano represented by concentration of ash with height. Most VATD models use a source of some prescribed shape calibrated against an empirical expression for the height-mass eruption rate (MER) relation. The actual vertical ash distribution in volcanic plumes usually varies from case to case and have complex dependencies on eruption source parameters and atmospheric conditions. We present here for the first time the use of a three-dimensional (3D) plume model to represent the ash cloud source without any assumption regarding plume geometry. By eliminating assumed behavior associated with a semiempirical plume geometry, the predictive skill of VATD simulations is greatly improved. To date, no VATD simulation adopts initial conditions created from first principles based on a 3D plume simulation. We use our recently developed volcanic plume model based on a 3D smoothed-particle hydrodynamic Lagrangian method, and couple the output to a standard Lagrangian VATD model. We apply the coupled model to the Pinatubo eruption in 1991 to illustrate the effectiveness of the approach. Our investigation reveals that initial particle distribution in the vertical direction has more impact on transport of ash clouds than does the horizontal distribution. Comparison with satellite data indicates that ash particles are concentrated through the depth of the volcanic umbrella cloud, and much lower than the observed maximum plume height.

Keywords: VATD, volcano, 3D plume model, initial conditions, numerical simulation, SPH, Pinatubo, ash transport, ash dispersal

1 INTRODUCTION

Volcanic ash, the fine-grained fraction of tephra, can be widely dispersed to synoptic and global scales, and can lead to a degradation of air quality and pose threats to aviation (Tupper et al., 2007). Identification, tracking and modeling the future movement of volcanic ash help route and schedule flights to avoid ash

24 clouds. Numerical estimation of ash distribution using known and forecast wind fields is necessary if we
25 are to accurately predict ash cloud propagation and spread. Numerous VATD models have been developed
26 by both civil and military aviation, and meteorological agencies to provide forecasts of ash cloud motion
27 (Witham et al., 2007), such as Puff (Tanaka, 1991; Searcy et al., 1998), VAFTAD (Heffter and Stunder,
28 1993), Tephra (Bonadonna et al., 2005), HYSPLIT(Stein et al., 2015; Rolph et al., 2017) and Ash3d
29 (Schwaiger et al., 2012). New techniques have been integrated into VATDs to satisfy increasing demands
30 for different types of output, model accuracy and forecast reliability. This contribution explores a method
31 for creating initial conditions for VATD simulations, which promises to reduce user inversion and hence
32 improve prediction capability.

33 Fero et al. (2009) and Stohl et al. (2011) showed that initial source conditions have significant effects
34 on simulation of volcanic ash transport. Besides location of the eruption vent and timings of the release,
35 traditional VATD simulation requires key global descriptors of the volcanic plume, especially plume height,
36 grain size, eruption duration and mass loading, or alternatively, a mass eruption rate (MER). No matter
37 how these global descriptors are obtained, they are used to furnish the initial conditions for VATDs in the
38 form of a line-source term of a spatio-temporal distribution of particle mass. It is a common practice to
39 pick values for these global descriptors using an empirical expression for the height-MER relation. The
40 values for the descriptors can also be found by parameter calibration (e.g. Fero et al., 2008, 2009; Stohl
41 et al., 2011; Zidikheri et al., 2017). One-dimensional (1D) plume models serve as an alternative option
42 to provide these values. For example, Bursik et al. (2012) used the 1D model puffin (Bursik, 2001) to
43 generate estimates of mass eruption rate and grain size. In some cases, an extra step is adopted to spread
44 ash particles from the line source horizontally, resulting in an initial ash cloud in 3D space. The horizontal
45 spreading depends on an empirical expression. For example, the VATD model Puff spreads particles from
46 the line source uniformly in the horizontal direction within a given radius. Considering the complexities of
47 volcanic eruptions, the actual ash distribution in the initial ash cloud should vary from case to case and with
48 time, making it difficult to find one general expression that is suitable for all cases. It is useful therefore to
49 investigate alternative ways for creating initial ash clouds without assumptions regarding plume geometry,
50 or numerical inversion. This provides the major motivation of this paper.

51 VATD models can be categorized into Lagrangian particle tracking and Eulerian advection-diffusion types.
52 Among several available particle tracking models, such as, Hypact (Walko et al., 1995), Puff (Searcy et al.,
53 1998), CANERM (D' amours, 1998), and HYSPLIT (Draxler and Hess, 1998) and advection-diffusion
54 models, such as, Tephra (Bonadonna and Houghton, 2005), Fall3D (Folch et al., 2009), and Ash3D
55 (Schwaiger et al., 2012), we adopt a particle tracking model, Puff, as the primary VATD model. Puff
56 can accept a 3D point cloud description of the starting ash cloud as an initial condition, which makes
57 it technically easier to couple with 3D plume models. Puff initializes a discrete number of tracers that
58 represent a sample of the eruption cloud, and calculates transport, turbulent dispersion, and fallout for each
59 representative tracer. A cylinder emanating vertically from the volcano summit to a specified maximum
60 height is the standard approach to provide a simple model of the geometry of a typical ash column. Puff
61 minimally requires horizontal wind field data. The “restart” feature of Puff makes it technically feasible to
62 accommodate the hand-off between a plume simulation and the Puff simulation in terms of time and length
63 scales. We also use the Hybrid Single-Particle Lagrangian Integrated Trajectory model (HYSPLIT) (Stein
64 et al., 2015; Rolph et al., 2017) to better understand simulation results from Puff in this study.

65 Besides parameter calibration, 1D plume models have been used to obtain global descriptors of volcanic
66 plumes. 1D plume models (e.g. Woods, 1988; Bursik, 2001; Mastin, 2007; de'Michieli Vitturi et al., 2015;
67 Folch et al., 2016; Pouget et al., 2016b) solve the equations of motion in 1D using simplifying assumptions,

and hence depend on estimation of certain parameters, especially those related to the entrainment of air, which is evaluated based on two coefficients: a coefficient due to turbulence in the rising buoyant jet, and one due to the crosswind field. Different 1D models adopt different entrainment coefficients based on a specific formulation or calibration against well-documented case studies. The feedback from plume to atmosphere is usually ignored in 1D models. While these 1D models generated well-matched results with 3D models for plumes that are dominated by wind (often called weak plumes) much greater variability is observed for strong plume scenarios (Bursik et al., 2009; Costa et al., 2016). On the other hand, 3D numerical models for volcanic plumes based on first principles and having few parametrized coefficients (Oberhuber et al., 1998; Neri et al., 2003; Suzuki et al., 2005; Cerminara et al., 2016a; Cao et al., 2018) naturally create a 3D ash cloud, which could serve directly as an initial state of the volcanic material for VATDs. However, there is no VATD simulation using such 3D ash clouds as initial conditions. In this paper, we will carry out VATD simulations using an initial state for the ash cloud based on 3D plume simulations, generated with Plume-SPH (Cao et al., 2018, 2017). The implementation techniques described in this paper can be applied to any combination of VATD model and 3D plume model even though our investigation is based on a specific VATD model and plume model.

The 1991 eruption of Pinatubo volcano is used as a case study. Pinatubo erupted between June 12 and 16, 1991, after weeks of precursory activity. The climactic phase started on June 15 at 0441 UTC and ended around 1341 UTC (Holasek et al., 1996a). The climactic phase generated voluminous pyroclastic flows, and sent Plinian and co-ignimbrite ash and gas columns to great altitudes (Scott et al., 1996). The evolution of the Pinatubo ash and SO₂louds was tracked using visible (Holasek et al., 1996a), ultraviolet (Total Ozone Mapping Spectrometer; TOMS) (Guo et al., 2004a) and infrared sensors, including the Advanced Very High-Resolution Radiometer (AVHRR) (Guo et al., 2004b). There is sufficient observational data to estimate the eruption conditions for the climactic phase of the eruption (Suzuki and Koyaguchi, 2009). The availability of calibrated eruption conditions and extensive observational data regarding ash cloud transport make the Pinatubo eruption an ideal case study.

2 MATERIALS AND METHODS

2.1 Plume-SPH Model

Plume-SPH (Cao et al., 2018) is designed to describe an injection of well mixed solid and volcanic gas from a circular vent above a flat surface into a stratified stationary atmosphere. The basic assumptions of the model are:

1. Molecular viscosity and heat conduction is neglected since turbulent energy and momentum exchange are dominant.
2. Erupted material consisting of solid with different size and mixture of gases is assumed to be well mixed and behave like a single phase fluid (phase 2) which is valid for eruptions with fine particles and ash.
3. Air, which is assumed to be well mixed mixture of different gases, is assumed to be another phase (phase 1).
4. Assume thermodynamic equilibrium and dynamic equilibrium between the two phases. As a result, both phases share the common energy equation and momentum equations.
5. All other microphysical processes (such as the phase changes of H₂O aggregation, disaggregation, absorption of gas on the surface of solids, solution of gas into a liquid) and chemical processes are not considered in this model.

109 6. The effect of wind, is also not yet considered in this model.

Based on above assumptions, the governing equations of our model are given as:

$$\frac{\partial \rho}{\partial t} + \nabla \cdot (\rho \mathbf{v}) = 0 \quad (1)$$

$$\frac{\partial \rho \xi}{\partial t} + \nabla \cdot (\rho \xi \mathbf{v}) = 0 \quad (2)$$

$$\frac{\partial \rho \mathbf{v}}{\partial t} + \nabla \cdot (\rho \mathbf{v} \mathbf{v} + p \mathbf{I}) = \rho \mathbf{g} \quad (3)$$

$$\frac{\partial \rho E}{\partial t} + \nabla \cdot [(\rho E + p) \mathbf{v}] = \rho \mathbf{g} \cdot \mathbf{v} \quad (4)$$

110 where ρ is the density, \mathbf{v} is the velocity, ξ is the mass fraction of ejected material, \mathbf{g} is the gravitational
 111 acceleration, \mathbf{I} is a unit tensor. $E = e + K$ is the total energy which is a summation of kinetic energy K
 112 and internal energy e . An additional equation is required to close the system. In this model, the equation
 113 for closing the system is the following equation of state (EOS).

$$p = (\gamma_m - 1) \rho e \quad (5)$$

114 where

$$\gamma_m = R_m / C_{vm} + 1 \quad (6)$$

$$R_m = \xi_g R_g + \xi_a R_a \quad (7)$$

$$C_{vm} = \xi_s C_{vs} + \xi_g C_{vg} + \xi_a C_{va} \quad (8)$$

$$\xi_a = 1 - \xi \quad (9)$$

$$\xi_g = \xi \cdot \xi_{g0} \quad (10)$$

$$\xi_s = \xi - \xi_g \quad (11)$$

120 where, C_v is the specific heat with constant volume, R is the gas constant. ξ is the mass fraction of erupted
 121 material. The subscript m represents mixture of ejected material and air, s represents solid portion in the
 122 ejected material, g represents gas portion in the ejected material, a represents air, 0 represents physical
 123 properties of erupted material. ξ_{g0} is the mass fraction of vapor in the erupted material.

124 Three different boundary conditions are applied in this model. At the vent, temperature of erupted
 125 material T , eruption velocity \mathbf{v} , the mass fraction of vapor in erupted material ξ_{g0} and mass discharge
 126 rate \dot{M} are given. The pressure of erupted material p is assumed to be the same as ambient pressure for
 127 pressure-balanced eruption. The radius of vent is determined from ρ , \dot{M} and \mathbf{v} . Non-slip wall boundary
 128 condition is applied to the flat ground, where we enforce the velocity to be zero. With further assumption
 129 that the ground is adiabatic, internal energy flux, which consists of heat flux and energy flux carried by
 130 mass flux, vanishes on the wall boundary. Pressure outlet boundary condition is applied to the surrounding
 131 atmosphere where the pressure is given. Except for the pressure, boundary values for density, velocity, and
 132 energy are determined by numerical calculation naturally. The initial condition for Plume-SPH is created
 133 based on atmosphere profile before the eruption.

134 The governing equations, EOS, boundary conditions, and initial conditions establish a complete mathematical
 135 model. The model is then discretized using smoothed particle hydrodynamics (SPH) method (Gingold

136 and Monaghan, 1977). The computational domain is discretized by SPH particles. The current version,
 137 Plume-SPH (Cao et al., 2018) uses two types of SPH particles: 1) particles of phase 1 to represent ambient
 138 air, and 2) particles of phase 2 to represent erupted material. So before the eruption, the computational
 139 domain is fully occupied by particles of phase 1. During the eruption, particles of phase 2 are injected
 140 into the computational domain. The discretized model is then converted into computational software
 141 (Plume-SPH) based on a parallel data management framework (Cao et al., 2017).

142 The input parameters for Plume-SPH include the eruption condition at vent, the material properties, and
 143 atmosphere profile. The eruption parameters, material properties and atmosphere for the “Strong plume–no
 144 wind” case in the recent comparison study on eruptive column models (Costa et al., 2016) are adopted.
 145 Eruption conditions and material properties are listed in Table 2. Note that the density of erupted material
 146 at the vent and radius of the vent can be computed from the given parameters. The eruption pressure
 147 is assumed to be the same as the atmospheric pressure at the vent, hence is not given in the table. The
 148 vertical profiles of atmospheric properties were based on the reanalysis data from European Centre for
 149 Medium-Range Weather Forecasts (ECMWF) for the period corresponding to the climactic phase of the
 150 Pinatubo eruption.

151 Running of Plume-SPH essentially updates physics quantities, such as temperature, velocity, and the
 152 position of SPH particles in each time step. During Plume-SPH simulation, SPH particles of phase 2, which
 153 represent the erupted material, are injected from the eruption vent into the computation domain with an
 154 initial injection velocity. As they moving upwards, these particles will get mixed with SPH particles of
 155 phase 1, which represent the air, during the whole simulation. Their physics quantities get updated as well.
 156 After the simulation, the computation domain will be filled with SPH particles of both phase 1 and phase 2.
 157 Removing all SPH particles of phase 1 from the computation domain, all of the left SPH particles are these
 158 particles that represent the erupted material, which naturally forms a plume (see Fig. 1).

159 2.2 Puff and Initial Ash Cloud

160 Puff (Tanaka, 1991; Searcy et al., 1998) is a dynamic pollutant tracer model. the model is based on a 3D
 161 Lagrangian form of the fluid mechanics, in which the material transport is represented by the fluid motion,
 162 and diffusion is parameterized by a stochastic process of random walk. Here, the model is constructed by a
 163 sufficiently large number of Lagrangian tracer particles with a random variables $\mathbf{R}_i(t) = (x(t), y(t), z(t))$,
 164 where $i = 1 \sim M$, which represent position vectors of particles from the origin of the ash source at the
 165 time t . M is total number of Lagrangian tracer particles, a sample of all the ash particles.

$$\mathbf{R}_i(t + \Delta t) = \mathbf{R}_i(t) + \mathbf{W}(t)\Delta t + \mathbf{Z}(t)\Delta t + \mathbf{S}_i(t)\Delta t \quad (12)$$

166 Here, \mathbf{W} accounts for local wind advection, \mathbf{Z} is generated by Gaussian random numbers and accounts
 167 for turbulent dispersion, and \mathbf{S} is the terminal gravitational fallout velocity or settling speed, which depends
 168 on a tracer’s size.

169 To start a Puff simulation, it requires a collection of tracer particles as the initial condition. The tracer
 170 particles has three basic properties, age, size and position. The age of each particle is the elapsed time
 171 from when they were released from the site. Ash particles in the initial ash cloud has zero ages. Ash size
 172 distribution is initialized using a Gaussian shape on a logarithmic scale. According to mean and standard
 173 deviation provided by user, Puff assigns size to each particle. Puff initialize the position of each particle
 174 according to semiempirical expressions. The height of each particle is determined according to specified
 175 distribution from the surface (1000 mbar $\cong 0$ m) to the top of the plume height, H_{max} , which is given

176 by user. Puff also supports reading predefined initial ash cloud from a file, contains the coordinates of all
 177 tracer particles.

178 The commonly used vertical particle distribution in Puff is the Poisson distribution. For the Poisson
 179 distribution, the vertical height of ash particles is given by Eq. (13):

$$H = H_{max} - 0.5H_{width} * P + H_{width}R \quad (13)$$

180 where P is an integral value drawn from a Poisson distribution of unit mean, R is a uniformly distributed
 181 random number between 0 and 1, H_{max} is the maximum plume height, H_{width} represents an approximate
 182 vertical range over which the ash will be distributed. So for Poisson distribution, user can specify two
 183 parameters, H_{max} and H_{width} . Another commonly used vertical ash distribution in VATD simulation is
 184 Suzuki. For the Suzuki plume shape (Suzuki et al., 1983), the ash mass vertical distribution is assumed to
 185 follow the Eq. (Eq. (14)):

$$Q(z) = Q_m * \frac{k^2(1 - z/H_{max})\exp(k(z/H_{max} - 1))}{H_{max} [1 - (1 + k)\exp(-k)]} \quad (14)$$

186 Where Q_m is the total mass of erupted material, k is shape factor, which is an adjustable constant that
 187 controls ash distribution with height. A low value of k gives a roughly uniform distribution of mass with
 188 elevation, while high values of k concentrate mass near the plume top. So for Suzuki distribution, besides
 189 the plume height H_{max} , there is another user specified parameter, k .

190 Puff initialize the horizontal distribution of ash particles according to semiempirical expression as well.
 191 Puff uses a uniformly distributed random process to determine ash particle locations in a circle centered
 192 on the volcano site. The maximum radius (at plume top) at which a particle can be located is given as
 193 “horizontal spread”. The horizontal displacement from a vertical line above the volcano is a random value
 194 within a circle of which the radius equals the “horizontal spread” multiplied by the ratio of the particle
 195 height H to the maximum H_{max} , see Eq. 15. So the resulting shape of the particle distribution within the
 196 plume is an inverted cone in which particles are located directly over the volcano at the lowest level and
 197 extend out further horizontally with increasing plume height.

$$r(H) = r_{max} * H/H_{max} * R \quad (15)$$

198 where $r(H)$ is the radius of the horizontal circle, whithin which, all particles at the height of H locate.
 199 r_{max} is the horizontal spread. H is the height, R is an uniformly distributed random number between 0 and
 200 1.

201 In summary, particle distributions in the initial ash cloud generated by semiempirical expressions are
 202 controlled by several parameters, for example, H_{max} , H_{width} , and r_{max} if user choose to use semiempirical
 203 expressions Eq. (13) and (15). User can optimize or calibrate these parameters to adjust the initial condition
 204 for Puff so that the simulated results match better with observations. Besides the initial ash cloud, other
 205 input parameters for Puff are diffusivity in the vertical and horizontal directions, start and end time of the
 206 eruption, and eruption duration. When creating initial conditions from output of Plume-SPH, the total
 207 number of Lagrangian tracers is the count of all SPH particles of phase 2 in the plume. The same total
 208 number of Lagrangian tracers are used when creating initial ash cloud based on semiempirical expressions.
 209 All input parameters for Puff are list in Table 3.

210 2.3 Creation of Initial Ash Cloud From Plume-SPH Output

211 In this study, we convert the output of Plume-SPH into initial ash cloud which serves as the initial
212 condition for Puff. The method proposed consists in generating the initial ash cloud directly from Plume-
213 SPH, foregoing assumptions and estimates, or inverse modeling, regarding ash injection height and timing.
214 The steps to create an initial ash cloud based on the raw output of Plume-SPH are shown in Fig. 1. The
215 initial ash cloud is created from SPH particles of phase 2, which represents the erupted material in the
216 model. After reaching the maximum rise height and starting to spread horizontally, particles of phase 2
217 form an initial umbrella cloud (Fig. 2). The 3D plume simulation is considered complete once the umbrella
218 cloud begins to form. Parcels that will be transported by the ambient wind are those above the “corner”
219 region, where mean plume motion is horizontal rather than vertical. With such consideration, we introduce
220 an elevation threshold, which is the lower elevation limit of the ash that will be transported by the VATD.
221 All SPH particles with elevation lower than the threshold are excluded when creating the initial ash cloud.
222 The inflection point from vertical raising to horizontal spreading happens around 15 km according to the
223 averaged vertical velocity ((d) in Fig. 2) and horizontal velocity ((e) in Fig. 2)). Below this inflection
224 point, particle trajectories are primarily vertical in the stalk-like eruption column. Above this level, particle
225 trajectories are primarily horizontal, as they flow into the umbrella cloud gravity current. So we choose 15
226 km to be the elevation threshold in this study.

227 Considering that SPH particles are only discretization points, each is assigned a grain size according to a
228 given total grain size distribution (TGSD) (Paladio-Melosantos et al., 1996), and a concentration according
229 to the mass and volumetric eruption rate. The Plume-SPH discretization points are thus switched to Puff
230 Lagrangian tracer particles having grain sizes and concentrations. The coordinates of these tracer particles,
231 which are initially in the local Cartesian coordinate system of Plume-SPH, are converted into Puff’s global
232 coordinate system, which is given in terms of (*longitude, latitude, height*). Puff takes the initial ash
233 cloud, consisting of the collection of Lagrangian tracer particles with grain size and concentration, and
234 propagates from time t to time $t + \Delta t$ via solution to an advection/diffusion equation (Eq. (12)).

235 To summarize, there are four steps to create an initial ash cloud from the raw output of Plume-SPH:

- 236 1. filter by SPH particle type to select SPH particles that represent erupted material (phase 2)
- 237 2. filter by a mean velocity threshold to select the upper part (above the “corner” region) dominated by
horizontal transport
- 238 3. switch SPH discretization points to Lagrangian tracer particles, by assigning grain size to each particle
- 239 4. convert coordinates of the SPH Lagrangian tracers into the VATDs’ geographic coordinate system

241 The features of the volcanic plume and resulting initial ash cloud used in the case study are shown in Fig. 2.
242 It is important to point out that since both Plume-SPH and Puff are based on the Lagrangian method, there
243 is no extra step of conversion between an Eulerian grid and Lagrangian particles.

244 2.4 Puff Restart

245 The plume and ash transport models are run at different time scales and length scales. The spatial and
246 temporal resolutions of the plume simulations are much finer than those of the ash transport model. It takes
247 tens of minutes (600 s in this case) for the Pinatubo plume to reach a steady height. However the eruption
248 persisted for a few hours (9 hours for the climactic phase of Pinatubo eruption), and it may be necessary to
249 track ash transport for days following an eruption. At present, it is too computationally expensive to do 3D
250 plume simulations of several hours in real time. In order to handle the difference in time scale, we mimic
251 a continuing eruption with intermittent pulses releasing ash particles. In particular, we restart Puff at an

interval of 600 s, i.e., the physical time of the plume simulation to reach a steady height. At every Puff restart, we integrate the output of the last Puff simulation and Plume-SPH into a new ash cloud. This new ash cloud serves as a new initial condition with which to restart a Puff simulation. A sketch demonstrating the overall restart process is shown in Fig. (3). The total number of Lagrangian tracer particles used in Puff thus equals the summed number of particles in all releases. The total number of tracer particles is therefore no longer a user-selected parameter. Fero et al. (2008) proposed using more realistic time-dependent plume heights. We do not adopt that strategy here for simplicity, although the idea would be straightforward in execution, given time-dependent eruption conditions.

3 RESULTS

Transport of volcanic ash resulting from the Pinatubo eruption on June 15, 1991, is simulated using two different initial conditions. The first type of initial condition is created in a traditional way according to user specified parameters (H_{max} , H_{width} and r_{max}) and the semiempirical plume shape expressions (Eq. (??) and (15)). We use the observed plume height (40 km) and two other parameters assigned semiempirically (Bursik et al., 2012) (TO DO: Add more details). The second type of initial condition is created by the new method proposed in this paper. To create initial conditions using the new method described in this paper, the plume rise is simulated first by Plume-SPH. Then the initial ash cloud is obtained by processing the raw output of Plume-SPH following steps described in Sec. 2.3. Except for initial conditions, the simulation parameters that control the VATD simulation are the same for both simulations. Simulated ash transport results are compared against observations.

The simulation results using different initial conditions are compared with TOMS images and AVHRR BTD ash cloud map imagery (Fig. 6). The differences between simulated ash transport by the “Semiempirical initial cloud + Puff” and “Plume-SPH+ Puff” conditions are significant. The simulated ash concentration based on the initial conditions created from Plume-SPH is qualitatively closer to observation than that based on the semiempirical plume shape expression. At 23 hours and 31 hours after the beginning of the climactic phase, the “Plume-SPH + Puff” simulation generates ash footprints that are closer to observations, especially in forecasting the location where there is a high concentration of ash. The “Semiempirical initial cloud + Puff” simulation, however, forecasts an ash distribution more spatially restricted than observation. The location of the high concentration region is far northwest of observation. This is confirmed by the Figure of Merit in Space (FMS), which is 0.148 when for Plume-SPH results while 0.124 for Semiempirical initial cloud. This must mean (TO DO: Add more analysis), Around 55 hours after the beginning of the climactic phase, the disparity between observation and simulation becomes more obvious. Ash in the “Semiempirical initial cloud + Puff” simulation is located too far west of the observation, with a FMS value equals to . The high concentration area of the “Plume-SPH + Puff” simulation, even though closer to observation, has also propagated further down the wind direction than the observation. As expected, the FMSs go down to 1 and 2 for the “Semiempirical initial cloud + Puff” and “Plume-SPH+ Puff” respectively. The decreasing of FMSs as a function of time indicates the accumulation of simulation errors during the simulation.

(TO DO: Add more analysis regarding the elevation plot, analysis the results by considering the effect of wind field)

Except for the initial conditions, both simulations adopt the same parameters and wind field data. That is to say, the only difference between these two simulations is the initial distribution of ash parcels. The main difference between simulation results from the “Plume-SPH + Puff” and the “Semiempirical initial cloud +

293 Puff" runs can be directly attributed to the initial ash particle distribution, which we discuss in detail in the
294 following section.

295 3.1 Importance of Maximum Height (H_{max})

296 In this section, we discuss the vertical distribution of ash particles in the initial ash cloud. The majority of
297 volcanic ash particles are usually injected at an elevation lower than the maximum height. For instance,
298 Holasek et al. (1996a,b) reported the maximum Pinatubo plume height as ~ 39 km while the cloud heights
299 were estimated at ~ 20 - 25 km. Self et al. (1996) reported that the maximum plume height could have
300 been > 35 km, but that plume heights were $23 \sim 28$ km after ~ 15 - 16 hours. The neutral buoyancy
301 height of the Pinatubo aerosol cloud was estimated with different methods at: ~ 17 - 26 km (lidar) by
302 DeFoor et al. (1992), ~ 20 - 23 km (balloon) by Deshler et al. (1992), ~ 17 - 28 km (lidar) by Jäger (1992),
303 and ~ 17 - 25 km (lidar) by Avdyushin et al. (1993). Based on comparison between simulated clouds
304 with early infrared satellite imagery of Pinatubo, Fero et al. (2008) reported that the majority of ash was
305 transported between 16 km and 18 km. These observations make good physical sense, as particles are
306 concentrated near the intrusion height of the umbrella cloud, not near the plume top, because the plume top
307 is due to momentum overshoot. However, the empirical expressions for the height-MER relation, which
308 are commonly adopted to create initial conditions for VATD simulations, tend to place the majority of ash
309 particles closer to the top if one uses observed maximum height in the empirical expressions.

310 Here we investigate two commonly used plume shapes, the Poisson (see Eq. (13)) and Suzuki (see Eq.
311 (14)). Particle distributions (in terms of mass percentage or particle number percentage) in the vertical
312 direction in the initial ash cloud are shown in Fig. 7. In that figure, the vertical particle distribution based
313 on Plume-SPH output is compared with the vertical particle distribution created based on semiempirical
314 shape expressions. Both Poisson and Suzuki distributions in Fig. 7 take $H_{max} = 40$ km, which is close
315 to the reported observation of maximum height. When adopting the Poisson distribution, see (c) in Fig.
316 7, the majority of the particles are between 30 km ~ 40 km. Obviously, the Poisson function distributes
317 the majority of ash at a higher elevation than was observed (e.g. Fero et al., 2008). As for the Suzuki
318 distribution, (d) in Fig. 7, the majority of ash particles also occur in a range that is significantly higher
319 than 25 km. Note that in the plot (d), the Suzuki constant k is set to 4, which is commonly used for sub-
320 plinian and plinian eruption columns (Pfeiffer et al., 2005). As for initial ash clouds based on Plume-SPH
321 simulation, most ash particles are distributed between ~ 17 - 28 km, which matches well with observations.
322 The maximum height is also consistent with observation.

323 For the Poisson distributions, the ash particles cannot be lower without changing the maximum height. To
324 distribute the majority of ash particles at a lower elevation, the maximum height must be reduced to a value
325 smaller than the observed maximum height. Adjusting parameters such as maximum height in the empirical
326 expression is actually the traditional source term calibration method. A set of initial ash clouds using
327 different maximum heights based on the Poisson distribution is shown in Fig. 8. The maximum heights
328 adopted in plume shape expressions are not obtained from any plume model or observation of plume height,
329 but by *a posteriori* calibration to later-observed ash cloud transport heights. For Suzuki, adjusting the
330 Suzuki constant can adjust the distribution of ash particles in vertical direction. As shown in Fig. 7, when k
331 is equals to 1 (see (e)), the majority of ash particles are at a lower elevation than observation. With $k = 3$
332 and $k = 6$ (figure (g) and (h)), the majority of ash particles are at a higher elevation than observation. When
333 k is set to 2 (see (f)), we can see that the majority of ash particles are roughly distributed in the range 17 -
334 28 km. But the shape, does not look like a typical plume, as particles are more uniformly distributed in
335 the vertical direction. In addition, the Suzuki constant is different from typical value for sub-plinian and

336 plinian eruption columns (Pfeiffer et al., 2005), means we can not apply previously experiences into the
337 semiempirical expression here.

338 The ash clouds created by the Poisson distribution with different maximum heights are used as initial
339 conditions in Puff simulations, whose results are shown in Fig. 11. Except for the maximum height, all
340 other parameters for creating an initial ash cloud are the same as those in Table 3. Of course, the range
341 over which the majority of ash particles is located is lower when using lower maximum heights. Figure
342 11 thus shows that the maximum height has a significant influence on the ash transport simulation. When
343 the maximum height is 10 km, the high concentration area lags behind that observed. If the designated
344 maximum height is 35 km, the high concentration area propagates faster and is more spatially confined
345 than observed. When using a maximum height of ~ 41 km, the high concentration area propagates faster
346 and the footprint is narrower than in both observation and “Plume-SPH + Puff” simulation results (see
347 Fig. 6). The simulated high concentration area is closest to “Plume-SPH + Puff” simulation results when
348 assigning a maximum height of 30 km. The low-concentration front of the volcanic ash cloud propagates
349 faster than observed, and is located far west of the high concentration areas. A low concentration tail area
350 also appears in the simulation results while there is no such tail in the observed imagery, although this
351 could be the result of imagery calibration or sensitivity. Simulation results based on a calibrated maximum
352 height of 30 km show a footprint similar to those of “Plume-SPH + Puff”, although smaller in terms of
353 area. However, the initial ash cloud created by a Poisson distribution with maximum height around 20 km
354 generates the best match ash with observation. (TO DO: More analysis here) That is to say, a maximum
355 height lower than the real maximum height is required by the Poisson plume shape to distribute ash particles
356 at elevations comparable to the “true” ash distribution. Our hypothesis regarding the disparity between the
357 “Semiempirical initial cloud + Puff” simulations and observation is confirmed. Since the initial condition
358 of vertical ash distribution has such a dominant effect on VATD simulation, it is critical for the forecast
359 capability of VATD simulations to explore more accurate and adaptive ways for establishing the initial ash
360 distribution, especially methods that do not rely on *a posteriori* parameter calibration or inversion.

361 3.2 Effect of Vertical Spread (H_{width})

362 In the previous section, we explored the effects of adjusting the maximum height to change the vertical
363 ash distribution at the source. In this section, we investigate the importance of another parameter in the
364 semiempirical Poisson expression (Eq. (13)). We vary the “vertical spread”, H_{width} , in the range $\sim 3 - 10$
365 km. A set of initial ash clouds with different vertical spreads are shown in Fig. 8. Except for vertical spread,
366 all other parameters for creating an initial ash cloud are the same as those in Table 3. The vertical width of
367 the region within which the majority of ash particles are located becomes narrower when a smaller value
368 for the vertical spread parameter is used, but changing it has no obvious effect on the height at which the
369 largest fraction of ash particles is injected (essentially the height of a mode in ash distribution). The ash
370 clouds based on different vertical spread parameters are then used as initial conditions in Puff simulations.

371 The VATD results are shown in Fig. 11. Adjusting of the vertical spread changes particle distribution in
372 the vertical direction, and thus, not surprisingly, affects the VATD simulation results. None of the VATD
373 simulations based on initial ash clouds with vertical spreads equal to 3, 5 or 10 km yield better results than
374 do VATD simulations based on initial conditions created by Plume-SPH (see Fig. 11).

375 The calibration tests on vertical spread, carried out here, are certainly not exhaustive. One could do a more
376 comprehensive calibration throughout the multi-dimensional parameter space (for Poisson distribution,
377 the parameter space is two dimensional) and find better results. In addition, with a more complicated
378 semiempirical plume shape expression, one could have more control over plume shape and might be able
379 to get an initial condition that yields a more accurate ash transport forecast. However, more complicated

380 and adaptable plume shape expressions imply a higher dimensional parameter space, which requires more
381 effort in calibration, even though the degrees of freedom to adjust plume shape are still limited. Creating
382 initial conditions based on 3D plume simulations is more adaptive to various cases and yields results as
383 good as or better than calibration of the poorly-constrained semiempirical parameter, vertical spread.

384 3.3 Horizontal Ash Distribution

385 The differences between the semiempirical plume particle distribution and actual (or simulated by the
386 3D plume model) are not only in the vertical direction. The importance of the horizontal distance of each
387 initial ash particle from a line extending upward from the volcano is investigated in this section. Puff uses a
388 uniformly distributed random process to determine ash particle locations in a circle centered on the volcano
389 site as described in section 2.2. For the output of Plume-SPH, an effective (maximum) radius is determined
390 according to a given threshold of ash concentration, following Cerminara et al. (2016b). A time averaged,
391 spatial integration of the dynamic 3D flow field is conducted to remove significant fluctuations in time and
392 space. Fig. 9 compares radius of the initial ash clouds created by 3D plume simulations with that assumed
393 in the semiempirical plume shape expression adopted in Puff. It is impossible for the simple, assumed
394 plume shapes to capture the complex and more realistic shapes developed by Plume-SPH. Additional
395 parameterization may generate more reasonable shapes, but these would continue to be *ad hoc*, none would
396 likely to have the potential fidelity of the 3D simulation to reality, and adding a temporally changing
397 distribution would be difficult.

398 Comparison between cross-sectional views of the initial ash clouds is shown in Fig. 10. The cross-
399 sectional view of horizontal particle distribution using the semiempirical method (last figure in Fig. 10)
400 is similar to a cross-sectional view of a simulated 3D plume, in a general sense. However, for simulated
401 3D plumes, the ash particle distribution in cross section varies with height, which factor would become
402 increasingly important with increasing wind speed, were wind speed to be included in the estimate of initial
403 plume shape. It is difficult for the semiempirical expressions to accommodate such a complex distribution.

404 Despite the obvious difficulty of correctly estimating ash distribution near the vent, or for short propagation
405 times, assigning different values for the horizontal spread has a negligible effect on VATD simulation
406 results at large time. We investigated horizontal spread values between 50 km and 1600 km to create initial
407 ash clouds; all of them generated similar results at large propagation times (> 1 day). Figure 11 shows
408 two different simulation results based on initial ash clouds with horizontal spread equal to 50 km and 600
409 km, respectively. No visible differences are apparent between them. (TO DO: add FMS comparison) This
410 implies that horizontal distribution has a less significant influence on VATD simulation results than does
411 vertical distribution for long distance or large time. Perhaps the most important ramification of this result
412 is that it means the time at which the “handshake” is made between Plume-SPH and the VATD does not
413 affect results significantly for relatively large distances and times.

4 DISCUSSION

414 4.1 Sensitivity of Other Inputs Parameters

415 Besides the initial ash cloud, other parameters for Puff simulations are: horizontal diffusivity, vertical
416 diffusivity, mean grain size, grain size standard deviation and total number of tracers. We present in this
417 subsection informal sensitivity studies on these parameters. We also investigate the influence of eruption
418 duration. The sensitivity analyses will serve as the basis for identifying possible sources of disparities
419 between simulation and observation.

420 Fero et al. (2008) simulated the volcanic ash transportation of Pinatubo eruption in 1991, he carried out
421 systematic sensitivity analysis with respect to input parameters of Puff and found that all other parameters

422 except for the plume height have negligible effect on long term ash transportation of Pinatubo. Inspired by
423 Fero et al. (2008), we carried out similar informal sensitivity analysis with much fewer sample points in
424 the parameter space and get similar results. Among the parameters explored, the eruption duration and
425 beginning time show the most obvious influence on simulated ash distribution, although the effect is still
426 small. To show the differences in an intuitive way, (a) - (c) in Fig. 4 shows simulated ash distribution
427 corresponding to 4.9 hours duration, 9 hours duration and 11 hours duration, respectively. After 72 hours,
428 relative to the simulation starting time, these three cases generate very similar results with tiny visible
429 differences (TO DO: The FMS values are , respectively). Daniele et al. (2009) did sensitivity analysis with
430 respect to the input parameters of Puff on different volcanos and found that for eruptive eruptions, the most
431 dominant factors are the wind field and plume height, while all other input parameters are relatively less
432 important. The significance of wind field has been confirmed by other researchers (Stefanescu et al., 2014,
433 e.g) as well.

434 We conducted several simulations with eruption duration varying in the range of [5, 11] hours with
435 slightly different starting time of climactic phase. Table 1 lists all these simulations. However, only slight
436 visible differences are observed among the simulated ash transport outputs. (TO DO: Add FMS value here).
437 We can see that the eruption duration has negligible effects on long-term ash transport.

438 The new methodology for generating initial ash clouds introduces a new parameter: elevation threshold,
439 which were specified based on averaged vertical velocity and horizontal velocity. We carry out a separate,
440 informal sensitivity analysis on this parameter by varying the elevation threshold from 1.5 km (the height
441 of the vent) to 25 m. The simulated ash distributions show obvious visible differences. Such influence
442 is especially obvious when the elevation threshold is either very high or very low. However, varying the
443 elevation threshold in the range of [12, 18] km generates relatively small differences in ash transport
444 simulation results. Figure 4 (d) and (e) compare the simulated ash distributions corresponding to elevation
445 thresholds of 1.5 km and 15 km. Compared with the ash distribution for a threshold of 15 km, an extra long
446 tail appears when using an elevation threshold of 1.5 km. Adopting lower elevation thresholds adds more
447 tracer particles at lower elevation. As the winds at different elevations are different, the tracers at lower
448 elevations propagate in different directions. The HYSPLIT (Stein et al., 2015; Rolph et al., 2017) forward
449 trajectory tracking starting at 1624 UTC on June 15, indicates that the wind between elevations of 10 km
450 and 15 km blew from north-east to south-west, while winds of higher elevation blew from east to west (see
451 Fig. 5). The results confirms that the elevation threshold is best estimated from the height the inflection
452 point in the vertical distribution (*cf.* Figure 4(d) and (e)).

453 4.2 Other Sources of Disparities

454 The full range of research issues raised by numerical forecasting of volcanic clouds is diverse. We focused
455 on the effect of initial conditions in this paper. During the plume modeling, seondary factors, such as
456 microphysical processes, even though they play lesser roles, likely need to be included to improve accuracy
457 for a particular eruption. Wind field are not considered in current version of Plume-SPH, but for weak
458 plume, wind plays such an important role that it has to be considered in the plume model. In addition,
459 eruption conditions are subject to change with time, even during the climactic phase of an eruption. In the
460 future, time-dependent initial conditions for VATDs can be created from 3D plume simulations based on
461 time-dependent eruption conditions. However, the eruption conditions at the vent are usually inferred from
462 observable information based on 1D plume models. Using 3D plume model won't reduce uncertainties
463 from the eruption conditions.

464 Assumption made in each VATD model is another source of errors. For example, a recent study by Osman
465 et al. (2020) demonstrated the great impact of GSD on modelled ash mass loadings using NAME(Jones

466 et al., 2007) to simulate historical eruptions of various VEIs. Other researchers (Beckett et al., 2015; Scollo
467 et al., 2008) have proven the significance of GSD using other VATD models. Their conclusion, however, is
468 different from our informal sensitivity study and other more comprehensive sensitivity studies using Puff.
469 This might be because of different assumptions made in different VATD models. These assumptions may
470 lead to underestimation or overestimation of certain factor, such as GSD.

471 One implicit assumption in the current method is that ash transportation is dominated by wind advection
472 (the passive dispersion approximation). However, during the growth of volcanic umbrella, the dominant
473 factors are various in different regimes (Pouget et al., 2016a) depending on characteristics of a particular
474 eruption. Webster et al. (2020) suggested that the lateral spread by the intrusive gravity current dominates
475 the transport of the ash cloud in this stage. A few studies by Larry Mastin (Mastin et al., 2014; Mastin
476 and Van Eaton, 2020) also showed that neglecting the umbrella cloud formation for larger eruptions led
477 to significantly different footprints for the resulting VATD fallout maps. Their studies imply that including
478 mapped velocities of the plume as a perturbation on the winds can better capture the radial spreading
479 of umbrella. In current method, the 3D plume model generated initial ash cloud has a radius around 25
480 km. For the Pinatubo 1991 eruption, the passive dispersion approximation can be reasonably applied
481 when radius is greater than 450 km, and can be fully valid only when the radius is greater than 1800 km
482 (Costa et al., 2013). It is computationally too expensive for Plume-SPH model to simulate an volcanic
483 umbrella. An umbrella model, with much coarse resolution, in between plume model and VATD model
484 would presumably better model the whole ash transportation process.

485 Besides the errors from assumptions of the model, errors are also introduced from the reanalysis wind
486 field data and the satellite observations, which are retrievals other than the truth.

487 4.3 Summary

488 This paper presents, for the first time, VATD simulations using initial source conditions created by a 3D
489 plume model. Traditional VATD simulations use initial conditions created according to a semiempirical
490 plume shape expression. A case study of the 1991 Pinatubo eruption demonstrates that a 3D plume model
491 can create more realistic initial ash cloud and ash parcel positions, and therefore improve the accuracy of
492 ash transport forecasts. Informal sensitivity analyses suggest that initial conditions, as expressed in the
493 disposition of initial ash parcel positions in the vertical, have a more significant effect on a volcanic ash
494 transport forecast than most other parameters. Comparison of initial ash parcel distributions among the
495 3D plume model, semiempirical expressions, and observations suggests that a major subpopulation of ash
496 parcels should be placed at a much lower elevation than maximum height to obtain a better VATD forecast.
497 For the Pinatubo case study, “well-matched” simulation results are observed when using a maximum height
498 of around 30 km in semiempirical expressions, which is much lower than the observed maximum height of
499 40 km. Comparing the effects of the maximum height, vertical spread and horizontal spread shows that ash
500 particle distribution in the vertical direction has the strongest effect on VATD simulation.

501 To summarize, we have presented a novel method for creating *a priori* initial source conditions for
502 VATD simulations. We have shown that it might be possible to obtain initial positions of ash parcels
503 with deterministic forward modeling of the volcanic plume, potentially obviating or lessening the need to
504 attempt to somehow observe initial positions, or *a posteriori* create a history of release heights via inversion
505 (Stohl et al., 2011). Although the method now suffers from the high computational cost associated with
506 3D forward modeling, there is the possibility that in future it might not only help overcome shortcomings
507 of existing methods used to generate *a priori* input parameters, but also overcome the need to do the
508 thousands of runs associated with inverse modeling. In addition, computational cost will continue to
509 diminish as computing speed increases. As they are forward numerical models based on first principles,

510 3D plume models need little if any parameterization, and user intervention should not be required to
511 improve forecast power; no assumption about the initial position of ash parcels is needed. Generation of the
512 initial cloud of ash parcels directly by 3D simulation is potentially adaptable to a variety of volcanic and
513 atmospheric scenarios. In contrast, semiempirical expressions used to determine initial conditions require
514 several parameters to control ash particle distribution along a vertical line source or some simplified shape
515 of the initial ash cloud, making it difficult in some cases to generate initial conditions that closely resemble
516 a complex reality.

CONFLICT OF INTEREST STATEMENT

517 The authors declare that the research was conducted in the absence of any commercial or financial
518 relationships that could be construed as a potential conflict of interest.

AUTHOR CONTRIBUTIONS

519 The idea of using 3D plume model to start a VATD simulation originated from a conversation between AP
520 and MB. ZC carried out the Plume-SPH simulations, Puff simulations, results analysis, and prepared the
521 first draft. All authors worked together for further revisions. MB carried out the HYSPLIT simulation. QY
522 post processed the Puff simulation results, overlapped the simulation results with satellite observation. All
523 authors contributed equally to the manuscript writing. AP and MB obtained funding to financially support
524 the work.

FUNDING

525 This work was supported by National Science Foundation awards 1521855, 1621853, and 1821311,
526 1821338 and 2004302 and by the National Research Foundation Singapore and the Singapore Ministry
527 of Education under the Research Centres of Excellence initiative (project number: NRF2018NRF-
528 NSFC003ES-010).

ACKNOWLEDGMENTS

529 We are grateful to the two anonymous reviewers of the paper for their constructive comments and suggestions
530 that improved the paper. Support for the Twentieth Century Reanalysis Project dataset is provided by
531 the U.S. Department of Energy, Office of Science Innovative and Novel Computational Impact on Theory
532 and Experiment (DOE INCITE) program, and Office of Biological and Environmental Research (BER),
533 and by the National Oceanic and Atmospheric Administration Climate Program Office.

REFERENCES

- 534 Avdyushin, S., Tulinov, G., Ivanov, M., Kuzmenko, B., Mezhuev, I., Nardi, B., et al. (1993). 1. spatial and
535 temporal evolution of the optical thickness of the pinatubo aerosol cloud in the northern hemisphere
536 from a network of ship-borne and stationary lidars. *Geophysical research letters* 20, 1963–1966
- 537 Beckett, F., Witham, C., Hort, M., Stevenson, J., Bonadonna, C., and Millington, S. (2015). Sensitivity of
538 dispersion model forecasts of volcanic ash clouds to the physical characteristics of the particles. *Journal
539 of Geophysical Research: Atmospheres* 120, 11–636
- 540 Bonadonna, C., Connor, C. B., Houghton, B., Connor, L., Byrne, M., Laing, A., et al. (2005). Probabilistic
541 modeling of tephra dispersal: Hazard assessment of a multiphase rhyolitic eruption at tarawera, new
542 zealand. *Journal of Geophysical Research: Solid Earth* 110
- 543 Bonadonna, C. and Houghton, B. (2005). Total grain-size distribution and volume of tephra-fall deposits.
544 *Bulletin of Volcanology* 67, 441–456

- 545 Bursik, M. (2001). Effect of wind on the rise height of volcanic plumes. *Geophys. Res. Lett* 28, 3621–3624
546 Bursik, M., Jones, M., Carn, S., Dean, K., Patra, A., Pavoloni, M., et al. (2012). Estimation and
547 propagation of volcanic source parameter uncertainty in an ash transport and dispersal model: application
548 to the eyjafjallajokull plume of 14–16 april 2010. *Bulletin of volcanology* 74, 2321–2338
549 Bursik, M., Kobs, S., Burns, A., Braitseva, O., Bazanova, L., Melekestsev, I., et al. (2009). Volcanic
550 plumes and wind: Jetstream interaction examples and implications for air traffic. *Journal of Volcanology*
551 and *Geothermal Research* 186, 60–67
552 Cao, Z., Patra, A., Bursik, M., Pitman, E. B., and Jones, M. (2018). Plume-sph 1.0: a three-dimensional,
553 dusty-gas volcanic plume model based on smoothed particle hydrodynamics. *Geoscientific Model*
554 *Development* 11, 2691–2715
555 Cao, Z., Patra, A., and Jones, M. (2017). Data management and volcano plume simulation with parallel
556 sph method and dynamic halo domains. *Procedia Computer Science* 108, 786–795
557 Cerminara, M., Esposti Ongaro, T., and Berselli, L. (2016a). Ashee-1.0: a compressible, equilibrium-
558 eulerian model for volcanic ash plumes. *Geoscientific Model Development* 9, 697–730
559 Cerminara, M., Esposti Ongaro, T., and Neri, A. (2016b). Large eddy simulation of gas–particle kinematic
560 decoupling and turbulent entrainment in volcanic plumes. *Journal of Volcanology and Geothermal*
561 *Research*
562 Costa, A., Folch, A., and Macedonio, G. (2013). Density-driven transport in the umbrella region of volcanic
563 clouds: Implications for tephra dispersion models. *Geophysical Research Letters* 40, 4823–4827
564 Costa, A., Suzuki, Y., Cerminara, M., Devenish, B., Esposti Ongaro, T., Herzog, M., et al. (2016). Results
565 of the eruptive column model inter-comparison study. *Journal of Volcanology and Geothermal Research*
566 D'amours, R. (1998). Modeling the etex plume dispersion with the canadian emergency response model.
567 *Atmospheric Environment* 32, 4335–4341
568 Daniele, P., Lirer, L., Petrosino, P., Spinelli, N., and Peterson, R. (2009). Applications of the puff model to
569 forecasts of volcanic clouds dispersal from etna and vesuvio. *Computers & Geosciences* 35, 1035–1049
570 DeFoor, T. E., Robinson, E., and Ryan, S. (1992). Early lidar observations of the june 1991 pinatubo
571 eruption plume at mauna loa observatory, hawaii. *Geophysical research letters* 19, 187–190
572 de'Michieli Vitturi, M., Neri, A., and Barsotti, S. (2015). Plume-mom 1.0: A new integral model of
573 volcanic plumes based on the method of moments. *Geoscientific Model Development* 8, 2447–2463
574 Deshler, T., Hofmann, D., Johnson, B., and Rozier, W. (1992). Balloonborne measurements of the pinatubo
575 aerosol size distribution and volatility at laramie, wyoming during the summer of 1991. *Geophysical*
576 *research letters* 19, 199–202
577 Draxler, R. R. and Hess, G. (1998). An overview of the hysplit_4 modelling system for trajectories.
578 *Australian meteorological magazine* 47, 295–308
579 Fero, J., Carey, S. N., and Merrill, J. T. (2008). Simulation of the 1980 eruption of mount st. helens using
580 the ash-tracking model puff. *Journal of Volcanology and Geothermal Research* 175, 355–366
581 Fero, J., Carey, S. N., and Merrill, J. T. (2009). Simulating the dispersal of tephra from the 1991
582 pinatubo eruption: implications for the formation of widespread ash layers. *Journal of Volcanology and*
583 *Geothermal Research* 186, 120–131
584 Folch, A., Costa, A., and Macedonio, G. (2009). Fall3d: A computational model for transport and
585 deposition of volcanic ash. *Computers & Geosciences* 35, 1334–1342
586 Folch, A., Costa, A., and Macedonio, G. (2016). Fplume-1.0: An integral volcanic plume model accounting
587 for ash aggregation. *Geoscientific Model Development* 9, 431
588 Gingold, R. A. and Monaghan, J. J. (1977). Smoothed particle hydrodynamics: theory and application to
589 non-spherical stars. *Monthly notices of the royal astronomical society* 181, 375–389

- 590 Guo, S., Bluth, G. J., Rose, W. I., Watson, I. M., and Prata, A. (2004a). Re-evaluation of so₂ release
591 of the 15 june 1991 pinatubo eruption using ultraviolet and infrared satellite sensors. *Geochemistry,*
592 *Geophysics, Geosystems* 5
- 593 Guo, S., Rose, W. I., Bluth, G. J., and Watson, I. M. (2004b). Particles in the great pinatubo volcanic cloud
594 of june 1991: The role of ice. *Geochemistry, Geophysics, Geosystems* 5
- 595 Heffter, J. L. and Stunder, B. J. (1993). Volcanic ash forecast transport and dispersion (vaftad) model.
596 *Weather and forecasting* 8, 533–541
- 597 Holasek, R., Self, S., and Woods, A. (1996a). Satellite observations and interpretation of the 1991 mount
598 pinatubo eruption plumes. *Journal of Geophysical Research: Solid Earth* 101, 27635–27655
- 599 Holasek, R. E., Woods, A. W., and Self, S. (1996b). Experiments on gas-ash separation processes in
600 volcanic umbrella plumes. *Journal of volcanology and geothermal research* 70, 169–181
- 601 Jäger, H. (1992). The pinatubo eruption cloud observed by lidar at garmisch-partenkirchen. *Geophysical*
602 *research letters* 19, 191–194
- 603 Jones, A., Thomson, D., Hort, M., and Devenish, B. (2007). The uk met office's next-generation
604 atmospheric dispersion model, name iii. In *Air pollution modeling and its application XVII* (Springer).
605 580–589
- 606 Mastin, L. G. (2007). A user-friendly one-dimensional model for wet volcanic plumes. *Geochemistry,*
607 *Geophysics, Geosystems* 8
- 608 Mastin, L. G. and Van Eaton, A. R. (2020). Comparing simulations of umbrella-cloud growth and ash
609 transport with observations from pinatubo, kelud, and calbuco volcanoes. *Atmosphere* 11, 1038
- 610 Mastin, L. G., Van Eaton, A. R., and Lowenstern, J. B. (2014). Modeling ash fall distribution from a
611 yellowstone supereruption. *Geochemistry, Geophysics, Geosystems* 15, 3459–3475
- 612 Neri, A., Esposti Ongaro, T., Macedonio, G., and Gidaspow, D. (2003). Multiparticle simulation of
613 collapsing volcanic columns and pyroclastic flow. *Journal of Geophysical Research: Solid Earth*
614 (1978–2012) 108
- 615 Oberhuber, J. M., Herzog, M., Graf, H.-F., and Schwanke, K. (1998). Volcanic plume simulation on large
616 scales. *Journal of Volcanology and Geothermal Research* 87, 29–53
- 617 Osman, S., Beckett, F., Rust, A., and Snee, E. (2020). Sensitivity of volcanic ash dispersion modelling to
618 input grain size distribution based on hydromagmatic and magmatic deposits. *Atmosphere* 11, 567
- 619 Paladio-Melosantos, M. L. O., Solidum, R. U., Scott, W. E., Quiambao, R. B., Umbal, J. V., Rodolfo, K. S.,
620 et al. (1996). Tephra falls of the 1991 eruptions of mount pinatubo. *Fire and mud* 12000, 12030
- 621 Pfeiffer, T., Costa, A., and Macedonio, G. (2005). A model for the numerical simulation of tephra fall
622 deposits. *Journal of Volcanology and Geothermal Research* 140, 273–294
- 623 Pouget, S., Bursik, M., Johnson, C. G., Hogg, A. J., Phillips, J. C., and Sparks, R. S. J. (2016a).
624 Interpretation of umbrella cloud growth and morphology: implications for flow regimes of short-lived
625 and long-lived eruptions. *Bulletin of Volcanology* 78, 1–19
- 626 Pouget, S., Bursik, M., Singla, P., and Singh, T. (2016b). Sensitivity analysis of a one-dimensional model
627 of a volcanic plume with particle fallout and collapse behavior. *Journal of Volcanology and Geothermal*
628 *Research*
- 629 Rolph, G., Stein, A., and Stunder, B. (2017). Real-time environmental applications and display system:
630 Ready. *Environmental Modelling & Software* 95, 210–228
- 631 Schwaiger, H. F., Denlinger, R. P., and Mastin, L. G. (2012). Ash3d: A finite-volume, conservative
632 numerical model for ash transport and tephra deposition. *Journal of Geophysical Research: Solid Earth*
633 117

- 634 Scollo, S., Folch, A., and Costa, A. (2008). A parametric and comparative study of different tephra fallout
635 models. *Journal of Volcanology and Geothermal Research* 176, 199–211
- 636 Scott, W. E., Hoblitt, R. P., Torres, R. C., Self, S., Martinez, M. M. L., and Nillos, T. (1996). Pyroclastic
637 flows of the june 15, 1991, climactic eruption of mount pinatubo. *Fire and Mud: eruptions and lahars of*
638 *Mount Pinatubo, Philippines*, 545–570
- 639 Searcy, C., Dean, K., and Stringer, W. (1998). Puff: A volcanic ash tracking and prediction model. *Journal*
640 *of Volcanology and Geothermal Research* 80, 1–16
- 641 Self, S., Zhao, J.-X., Holasek, R. E., Torres, R. C., and King, A. J. (1996). The atmospheric impact of the
642 1991 mount pinatubo eruption
- 643 Stefanescu, E., Patra, A. K., Bursik, M., Jones, M., Madankan, R., Pitman, E. B., et al. (2014). Fast
644 construction of surrogates for uq central to dddas—application to volcanic ash transport. *Procedia*
645 *Computer Science* 29, 1227–1235
- 646 Stein, A., Draxler, R., Rolph, G., Stunder, B., Cohen, M., and Ngan, F. (2015). Noaa's hysplit atmospheric
647 transport and dispersion modeling system. *Bulletin of the American Meteorological Society* 96, 2059–
648 2077
- 649 Stohl, A., Prata, A., Eckhardt, S., Clarisse, L., Durant, A., Henne, S., et al. (2011). Determination of
650 time-and height-resolved volcanic ash emissions and their use for quantitative ash dispersion modeling:
651 the 2010 eyjafjallajökull eruption. *Atmospheric Chemistry and Physics* 11, 4333–4351
- 652 Suzuki, T. et al. (1983). A theoretical model for dispersion of tephra. *Arc volcanism: physics and tectonics*
653 95, 113
- 654 Suzuki, Y. and Koyaguchi, T. (2009). A three-dimensional numerical simulation of spreading umbrella
655 clouds. *Journal of Geophysical Research: Solid Earth (1978–2012)* 114
- 656 Suzuki, Y. J., Koyaguchi, T., Ogawa, M., and Hachisu, I. (2005). A numerical study of turbulent mixing
657 in eruption clouds using a three-dimensional fluid dynamics model. *Journal of Geophysical Research:*
658 *Solid Earth* 110
- 659 Tanaka, H. (1991). Development of a prediction scheme for the volcanic ash fall from redoubt volcano. In
660 *First Int'l. Symp. on Volcanic Ash and Aviation Safety*. vol. 58
- 661 Tupper, A., Itikarai, I., Richards, M., Prata, F., Carn, S., and Rosenfeld, D. (2007). Facing the challenges of
662 the international airways volcano watch: the 2004/05 eruptions of manam, papua new guinea. *Weather*
663 and Forecasting 22, 175–191
- 664 Walko, R., Tremback, C., and Bell, M. (1995). Hypact: The hybrid particle and concentration transport
665 model. *User's guide*
- 666 Webster, H. N., Devenish, B. J., Mastin, L. G., Thomson, D. J., and Van Eaton, A. R. (2020). Operational
667 modelling of umbrella cloud growth in a lagrangian volcanic ash transport and dispersion model.
668 *Atmosphere* 11, 200
- 669 Witham, C., Hort, M., Potts, R., Servranckx, R., Husson, P., and Bonnardot, F. (2007). Comparison of
670 vaac atmospheric dispersion models using the 1 november 2004 grimsvötn eruption. *Meteorological*
671 *Applications* 14, 27–38
- 672 Woods, A. (1988). The fluid dynamics and thermodynamics of eruption columns. *Bulletin of Volcanology*
673 50, 169–193
- 674 Zidikheri, M. J., Lucas, C., and Potts, R. J. (2017). Estimation of optimal dispersion model source
675 parameters using satellite detections of volcanic ash. *Journal of Geophysical Research: Atmospheres*
676 122, 8207–8232

FIGURE CAPTIONS

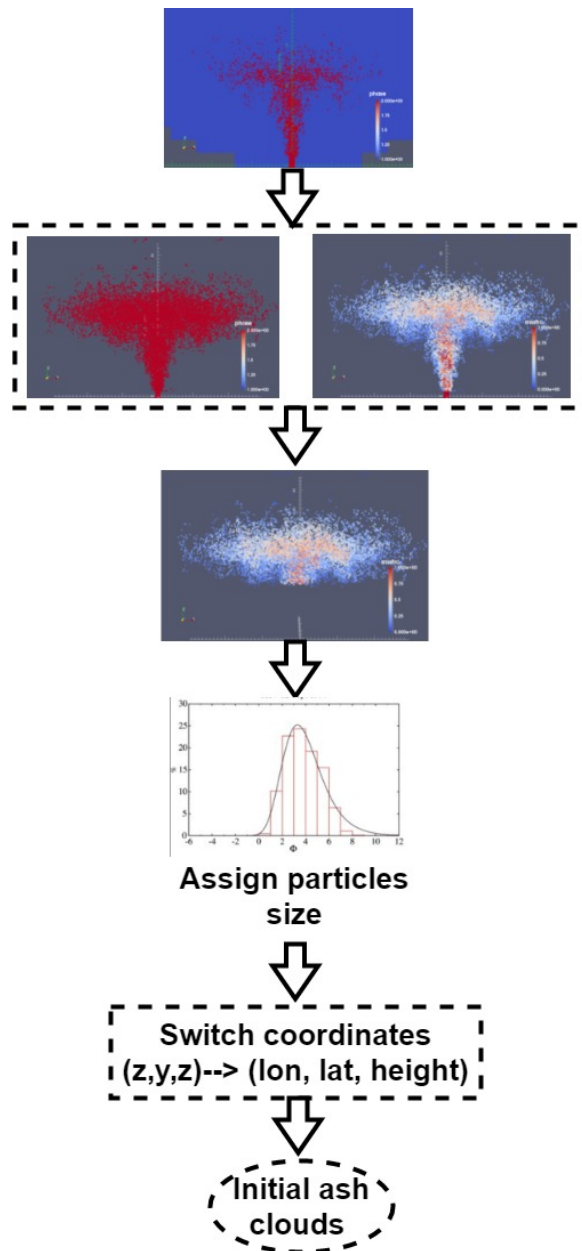


Figure 1. Steps to create initial condition for Puff based on raw output of Plume-SPH (Cao et al., 2018). First row: raw output of Plume-SPH. Blue particles are phase 1 (ambient air), red particles are phase 2 (erupted material). Second row: plume after removing SPH particles of phase 1. Picture at right is colored according to the mass fraction of erupted material. Third row: volcanic plume above the “corner” region after cutting off the lower portion. Fourth row: assign sizes to particles converting numerical discretization points into tracers. Fifth row: switch coordinates in local coordinate system into (*longitude, latitude, height*)

Table 1. The starting and ending time (UT) for simulating the climactic phase of Pinatubo eruption on June 15 1991. Observed plume height (Holasek et al., 1996a) at different time are also listed in the table.

Eruption duration	4.9 hours	9 hours	10 hours	11.1 hours
Start time	0441	0441	0441	0334
Height at start time	37.5 km	37.5 km	37.5 km	24.5 km
End time	0934	1341	1441	1441
Height at end time	35 km	26.5 km	22.5	22.5 km

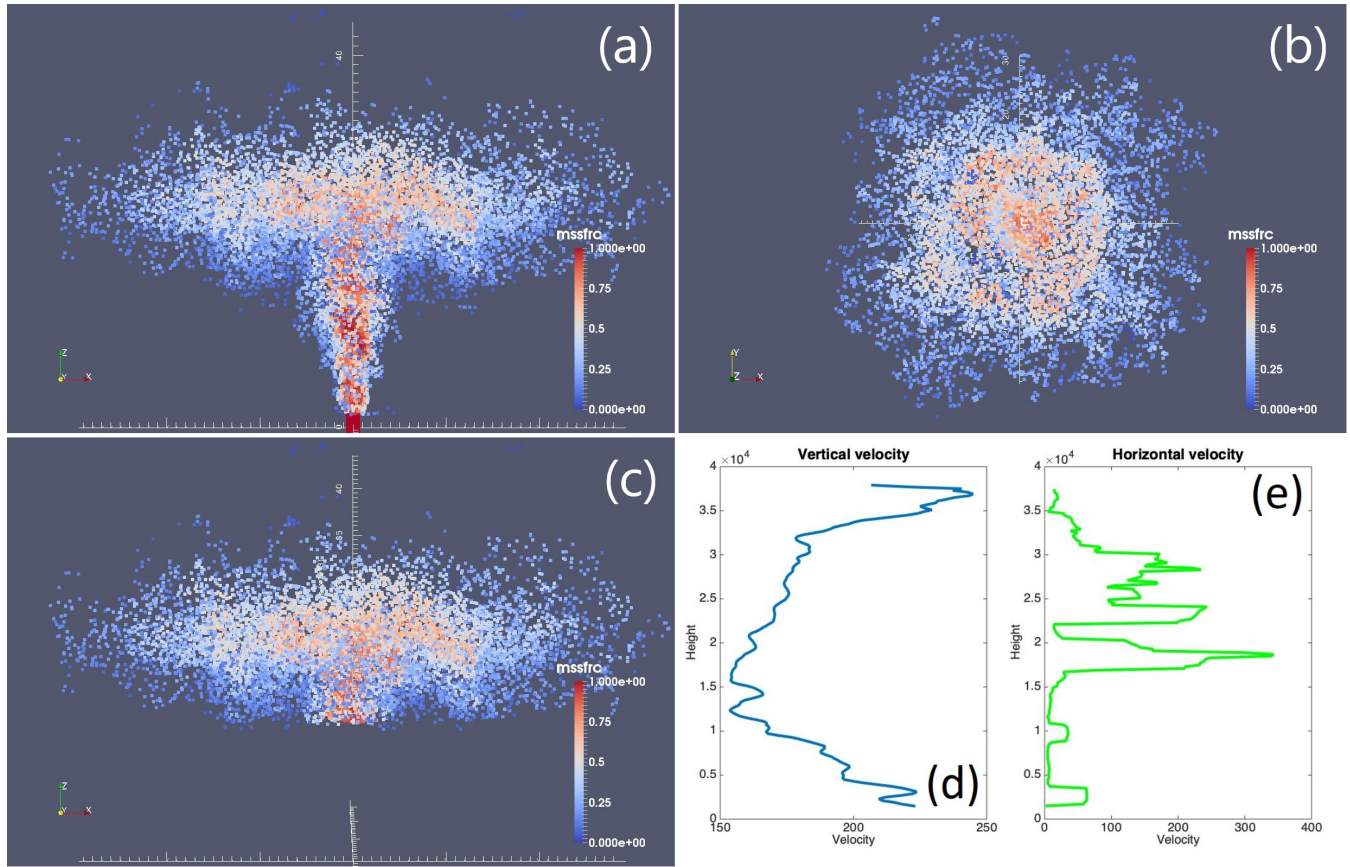


Figure 2. Volcano plume from 3D plume model. All particles in the pictures are of phase 2 (particle of phase 1 has been removed) at 600s after eruption, at which time, the plume has already reached the maximum height and started spreading radially. (a) is front view of the whole plume. (b) top view of the plume. (c) is front view of the initial ash cloud, which is essentially a portion of the whole plume with elevation higher than a given threshold (in this picture is 15000m). Particles are colored according to mass fraction of erupted material. Red represents high mass fraction while blue represents low mass fraction.

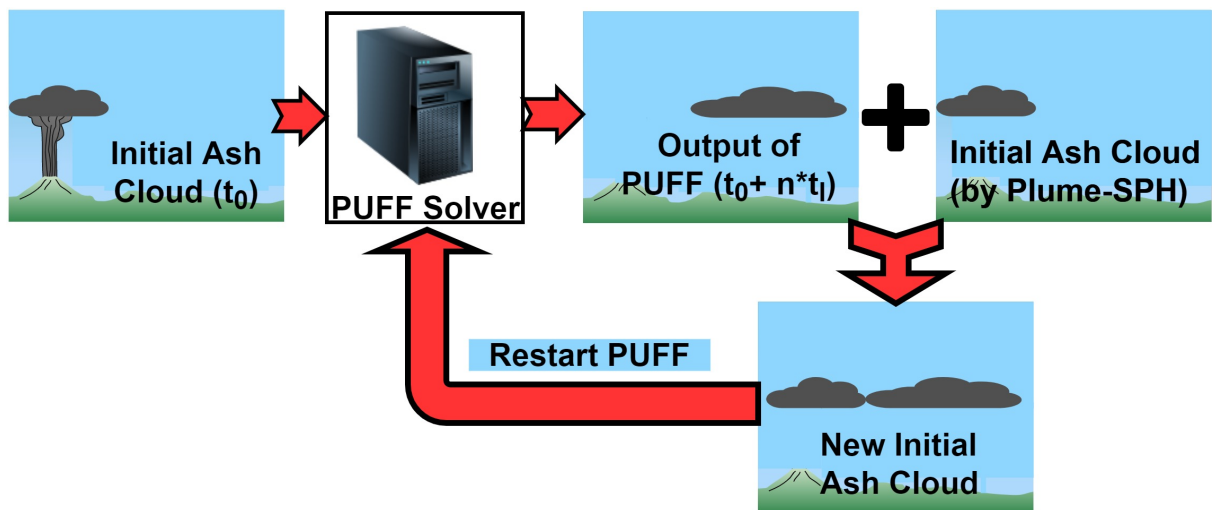


Figure 3. Mimic successive eruption with intermittent pulsed releasing of ash particles. t_I is the period of pulsing release. t_I equals the physical time of 3D plume simulation.

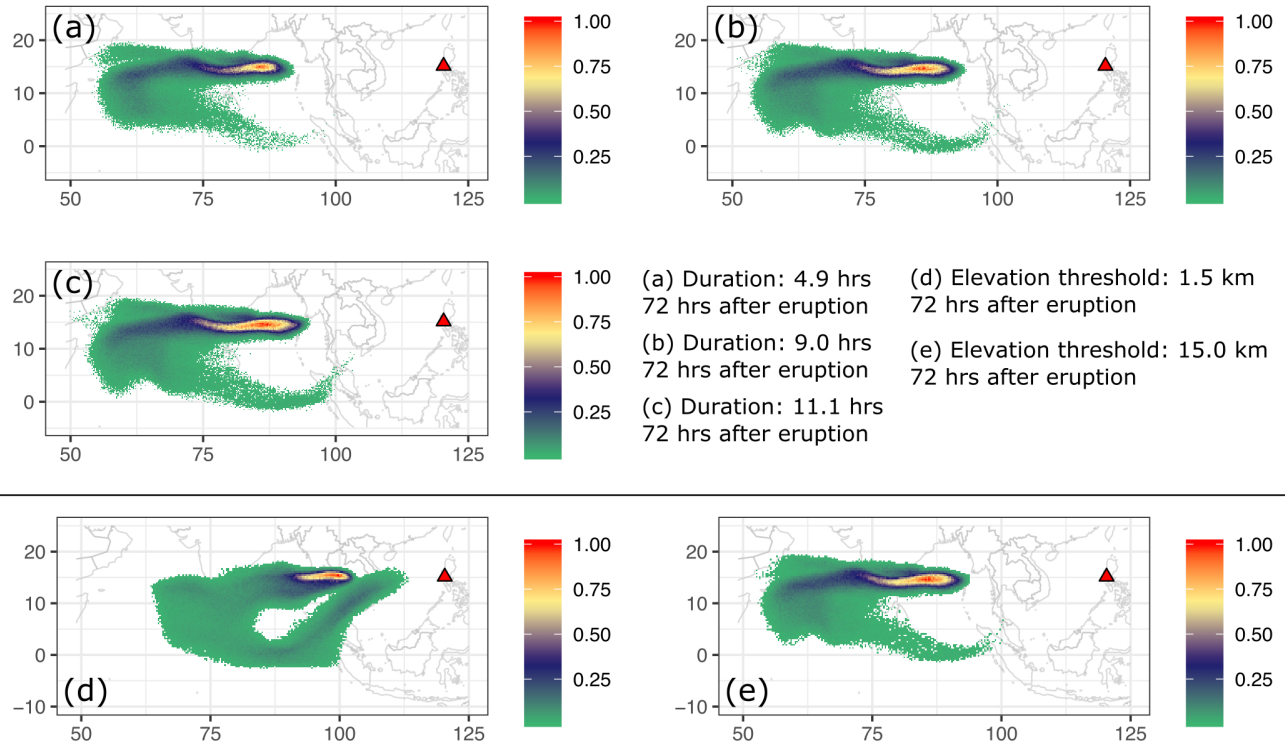


Figure 4. Sensitivity of Puff simulation with respect to eruption durations and initial ash cloud cutoff heights .(a) to (c) are simulated ash distribution with different starting and ending time. They corresponding to eruption duration of 4.9 hours, 9 hours and 11.1 hours respectively. Starting and ending time for each case is in Table 1. (d) and (e) are simulated ash distribution taking initial ash clouds obtained using different elevation thresholds (1500m and 15000 m) from output of Plume-SPH. The starting and ending time are corresponding to 9 hours duration case in Table 1. The contours correspond to ash concentration at 72 hours after eruption.

Table 2. List of eruption condition and material properties for plume simulation

Parameters	Units	Plume
Vent velocity	$m \cdot s^{-1}$	275
Vent gas mass fraction		0.05
Vent Temperature	K	1053
Vent height	m	1500
Mass discharge rate	$kg \cdot s^{-1}$	1.5×10^9
Specific heat of gas at constant volume	$J \cdot kg^{-1} \cdot K^{-1}$	717
Specific heat of air at constant volume	$J \cdot kg^{-1} \cdot K^{-1}$	1340
Specific heat of solid	$J \cdot kg^{-1} \cdot K^{-1}$	1100
Specific heat of gas at constant pressure	$J \cdot kg^{-1} \cdot K^{-1}$	1000
Specific heat of air at constant pressure	$J \cdot kg^{-1} \cdot K^{-1}$	1810
Density of air at vent height	$kg \cdot m^{-3}$	1.104
Pressure at vent height	Pa	84363.4

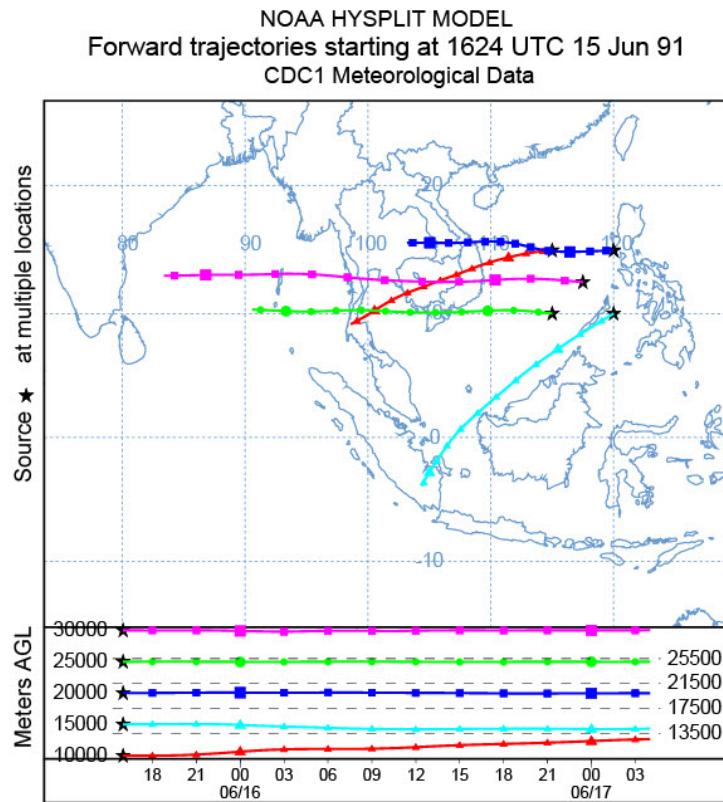


Figure 5. Trajectories of particles starting from different heights indicating the wind directions of different evaluations. The trajectories are chosen to start at points that were on the perimeter of the umbrella cloud in x , y and z , and in its center, right before it became affected by the wind to give an idea of the maximum possible spread of the trajectories from that initial condition.

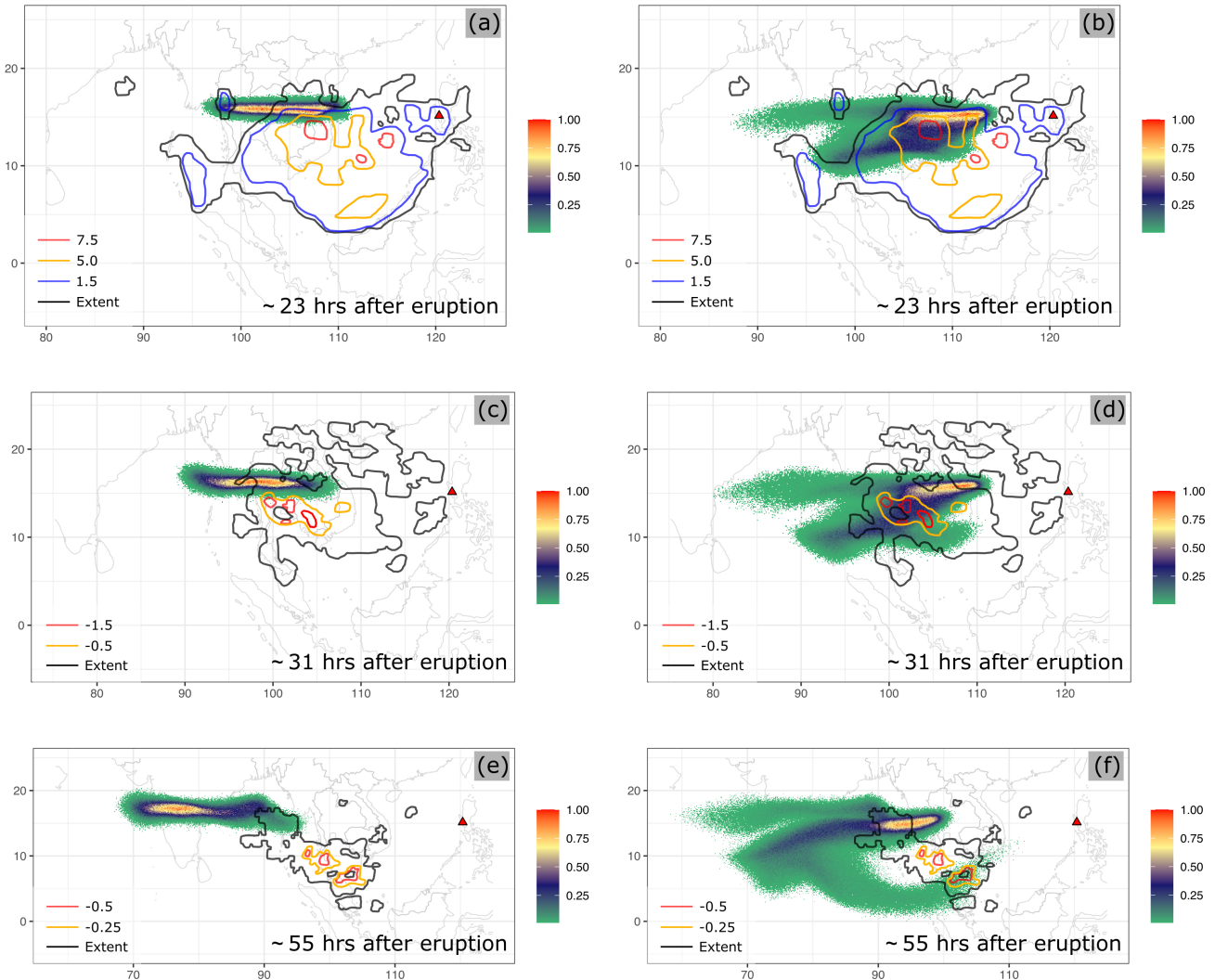


Figure 6. Comparison between “Semiempirical initial cloud + Puff” and “Plume-SPH + Puff”. Pictures to the left are: Puff simulation based on initial condition created according to semiempirical plume shape expression. Pictures to the right are Puff simulation based on initial condition generated by Plume-SPH. TOMS or AVHRR image of Pinatubo ash cloud are overlapped with the simulation results. Ash clouds at different hours after eruption are on different rows. From top to bottom, the images are corresponding to around 23 hours after eruption (UT 199106160341), 31 hours after eruption (UT 199106161141), 55 hours after eruption (UT 199106171141). The observation data on the first row are TOMS ash and ice map. The observation data on the second and third row are AVHRR BTD ash cloud map with atmospheric correction method applied (Guo et al., 2004b).

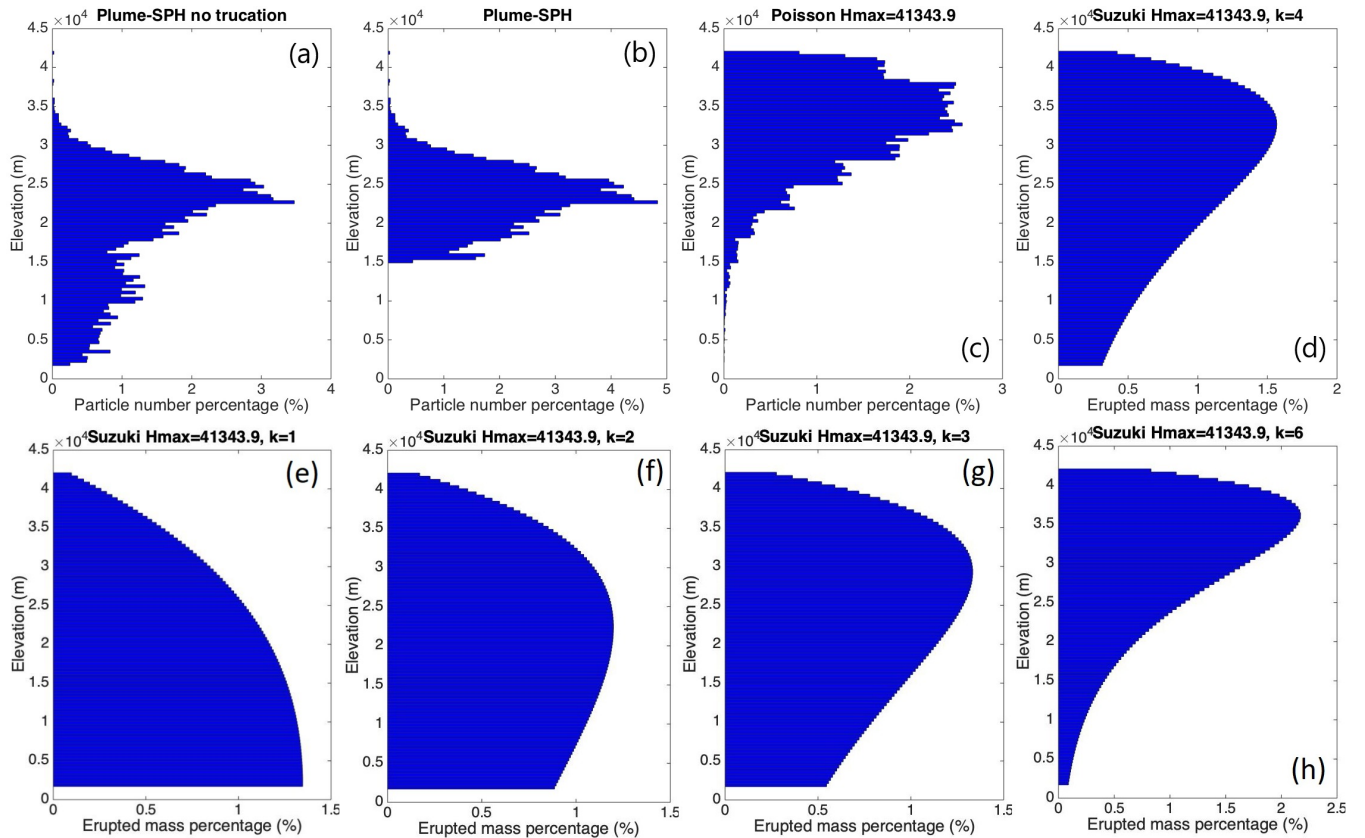


Figure 7. Particle distribution of initial ash cloud in vertical direction. (a) is corresponding to the initial ash cloud obtained from Plume-SPH output. (b) is corresponding to ash distribution of Plume-SPH output truncated by a elevation threshold of 15000m. (c) is for vertical ash distribution based on Poisson distribution with maximum height equals to 40000m. Another parameter, the vertical spread, in the expression of Poisson plume shape is 6662m. (d) is corresponding to Suzuki distribution with maximum height equals to 40000m. Another parameter in Suzuki distribution, the shape factor, is 4. The x axis is the percentage of particle numbers for Plume-SPH and Poisson. For Suzuki the x axis is the mass percentage of erupted material.

Table 3. Parameters used in VATD simulation of the climactic phase of Pinatubo eruption on June 15 1991. The first six parameters are used by semiempirical expression to create an initial ash cloud. When creating an initial condition based on the Plume-SPH model, these parameters are extracted from output of Plume-SPH model.

Parameters	Unit	Semiempirical	Plume-SPH
Maximum Height (H_{max})	m	40000	-
Horizontal Spread (r_{max})	km	103.808	-
Vertical Spread (H_{width})	km	6.662	-
Plume Shape	-	Poisson	-
Total Ash Particles	-	1768500	1768500
Elevation Threshold	m	-	15000
Horizontal Diffusivity	m^2/s	10000	10000
Vertical Diffusivity	m^2/s	10	10
Grain Size Distribution	-	Gaussian	Gaussian
Mean of Grain Size (Radius)	mm	3.5×10^{-2}	3.5×10^{-2}
Standard Deviation of Grain Size	-	1.0	1.0
Start Time	UT	0441	0441
End time	UT	1341	1341
Simulation Duration	hour	72	72

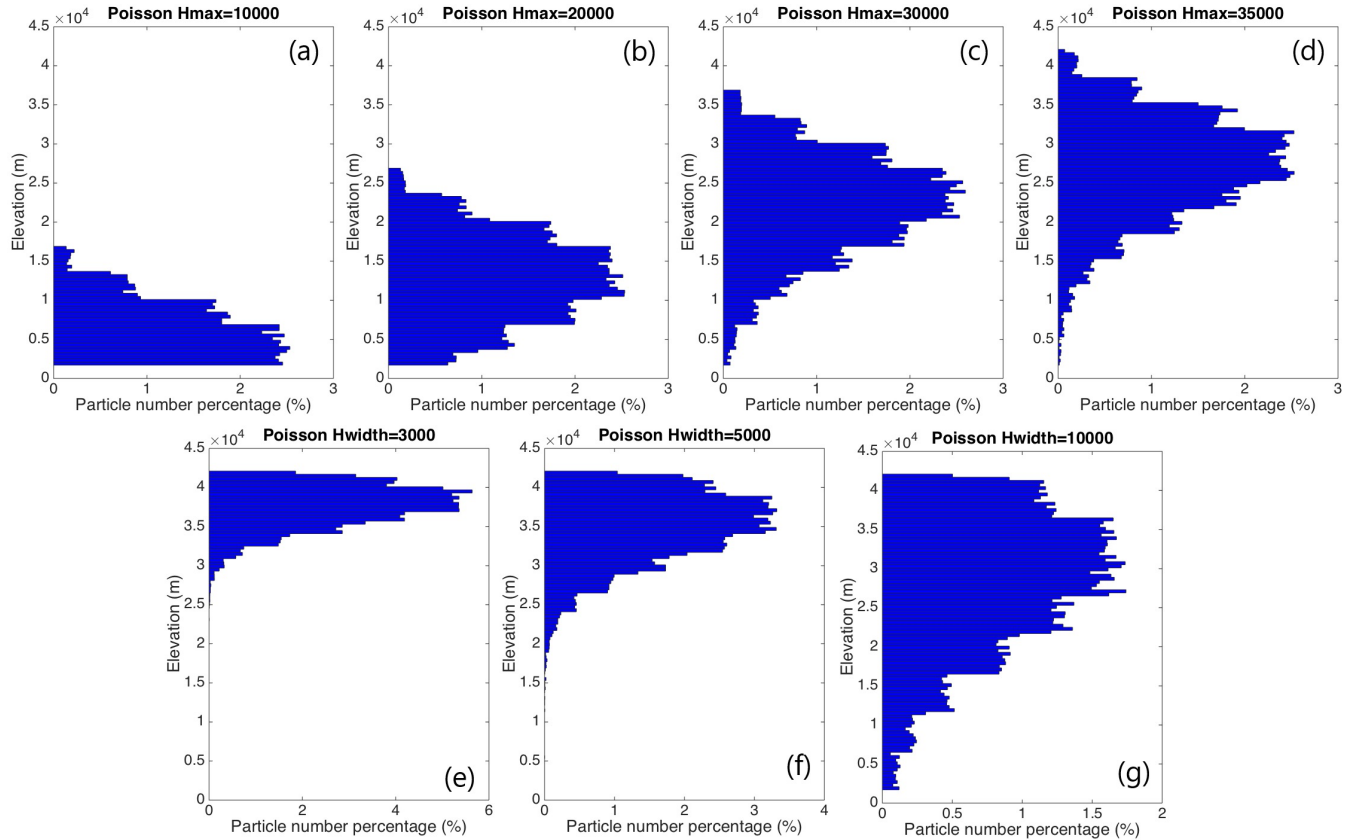


Figure 8. Initial particle distribution in vertical direction based on Poisson plume shape. The first row varies maximum heights. (a) to (d) are corresponding to maximum height of 10000m, 20000m, 30000m, 35000m. Another parameter, the vertical spread, in the expression of Poisson plume shape is 6662m for all four figures in the first row. The second row varies “vertical spread”. (e) to (g) are corresponding to vertical spread of 3km, 5km and 10km. The maximum height in the expression of Poisson plume shape is 40000m for all three figures. The x axis is the percentage of particle numbers. See Fig. 7 for vertical ash distribution of Plume-SPH output.

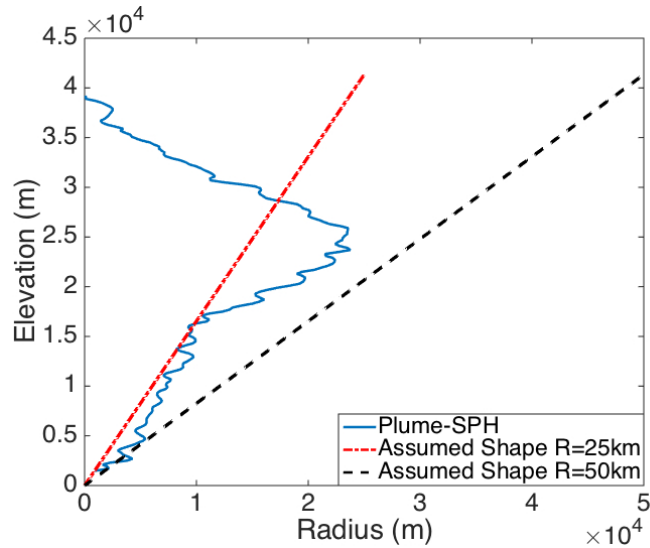


Figure 9. Comparison between radius of initial ash clouds created by 3D plume model (Plume-SPH) and assumed initial ash cloud shape in Puff. The plume shape expression used in Puff defines an inverted cone whose actual shape changes when “horizontal spread” takes different values. $R = 25\text{km}$ is corresponding to “horizontal spread” equals to 50km . $R = 50\text{km}$ is corresponding to “horizontal spread” equals to 100km

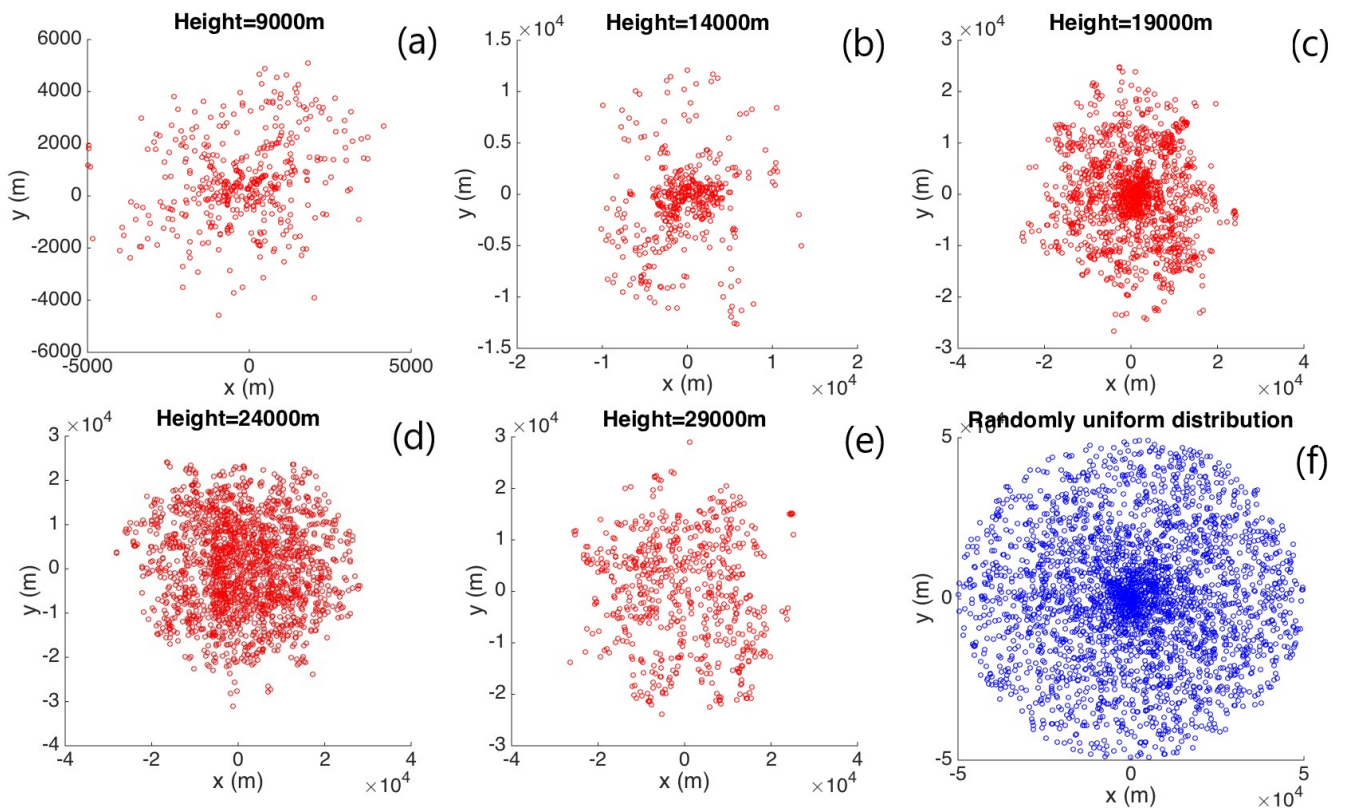


Figure 10. Horizontal distribution of ash particles (tracers) on a cross section of initial ash cloud. Puff assumes a randomly uniform distribution of ash particles within a circle, as shown by blue dots in (f). All other figures show the ash particle distribution of initial ash clouds created by Plume-SPH at different elevations.

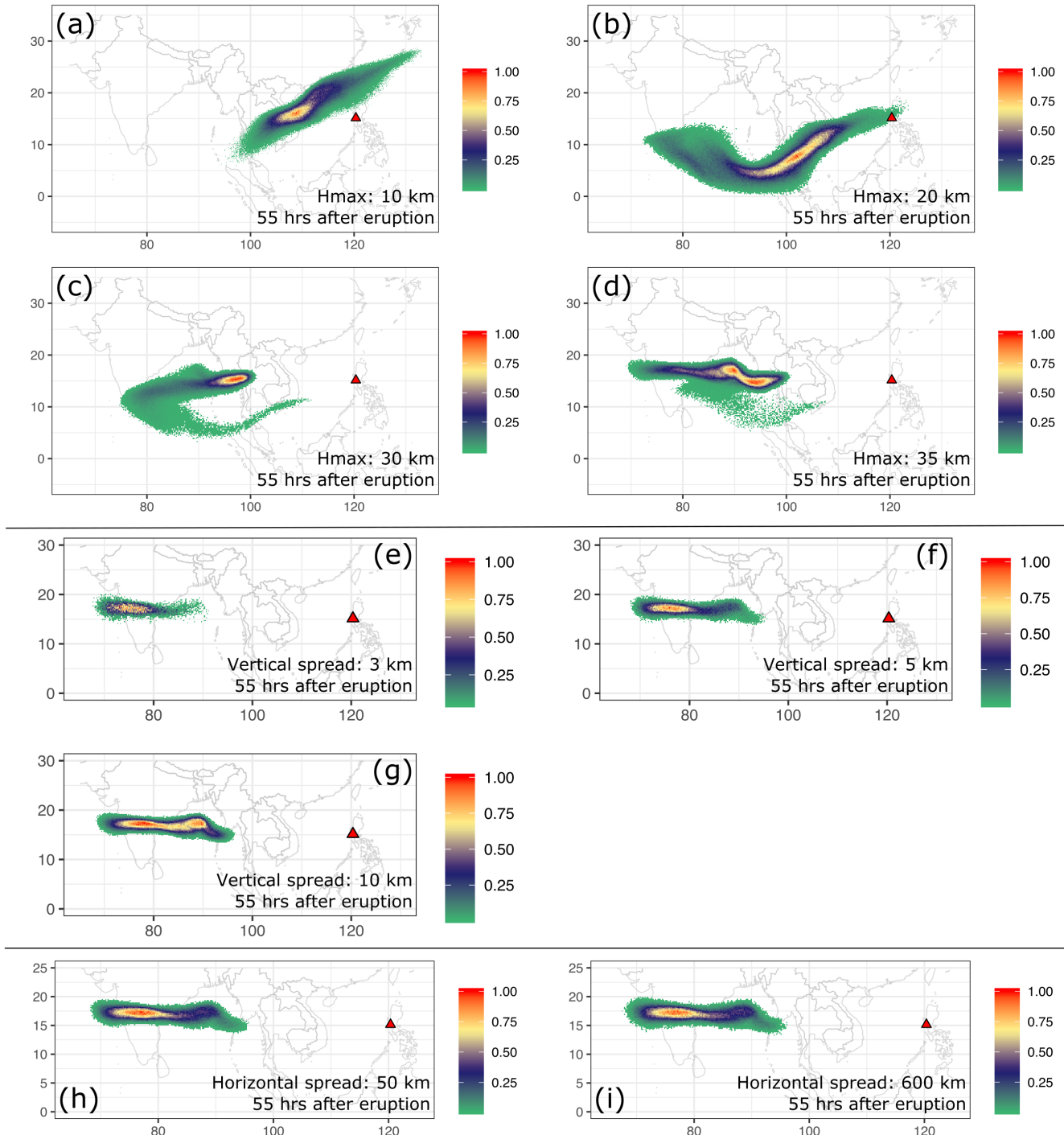


Figure 11. Ash transport simulated by Puff using different initial ash clouds created according the empirical expressions. Initial ash cloud for (a) to (d) are created according to Poisson distribution with maximum plume heights of 10km, 20km, 30km and 35km respectively. Initial ash cloud for (e) to (g) are created with vertical spread equals to 3km, 5km and 10km. respectively. Initial ash cloud for (h) - (i) are created with “horizontal spread” equals to 50km and 600km respectively. All images are for simulated ash transport around 55 hours after eruption (UT 199106171141). See the observed cloud image in Fig. 6.